Article

Beyond Hodgkin-Huxley—The Ionic-Mechano-Hydraulic (IMH) Model of Nerve Conduction

Bernard Delalande [*,†], Hirohisa Tamagawa [†], Vladimir Matveev [†]

Posted Date: 24 March 2026

doi: 10.20944/preprints202603.0725.v4

Keywords: nerve conduction; action potential; hydraulic wave; polyelectrolyte gel; Ling associationinduction hypothesis; Donnan equilibrium; myelin; saltatory conduction; Hofmeister series; mechanoreceptor; Umwelt; Hodgkin-Huxley model

 doi:10.20944/preprints202603.0725.v4

Article

Beyond Hodgkin-Huxley—The Ionic-Mechano-Hydraulic (IMH) Model of Nerve Conduction

Bernard Delalande [1,2,*,†], Hirohisa Tamagawa [2,†] and Vladimir Matveev [3,†]

[1] 280, avenue de la Pierre Dourdant, 38290 La Verpilliere, France
[2] Department of Mechanical Engineering, Faculty of Engineering, Gifu University, 1-1 Yanagido, Gifu, Gifu, 501-1193 Japan
[3] Laboratory of Cell Physiology, Institute of Cytology, Russian Academy of Sciences, Tikhoretsky Ave 4, St. Petersburg 194064, Russia
* Correspondence: bernard@somasimple.com
† These authors contributed equally to this work.

Abstract

The Hodgkin-Huxley (HH) model has dominated quantitative neuroscience since 1952. Its authors explicitly acknowledged its phenomenological character and called for a deeper mechanistic account. We propose that this account is the IMH model of nerve conduction. The model is based on three biophysical foundations: (1) the Ling polyelectrolyte gel framework, in which intracellular K^+ is adsorbed at protein sites and the resting ionic distribution is a Donnan equilibrium thermodynamically stable that does not require a metabolic pump [6,7]; (2) the Hofmeister ion series, which governs differential adsorption of K^+ versus Na^+ [8]; and (3) the hydraulic wave equation for a fluid-filled elastic tube, which predicts conduction velocity from myelin elastic modulus rather than sodium channel density. In this framework, the action potential is a coupled ionic-hydraulic phase transition propagating as a pressure wave in the periaxonal space. Electrical events are causally secondary – the electromagnetic shadow of the hydraulic wave, not its cause. We demonstrate that the model resolves a 75-year-old anomaly identified but left unexplained by Huxley and Stämpfli in 1949 [10]: positive current enters a node before the membrane potential reaches its maximum, a relation the authors themselves described as "impossible in a system of resistances and capacities." We present nine falsifiable predictions distinguishing the IMH model from HH, covering myelin mechanics, mechanoreceptor adaptation, terminal arborisation geometry as the physical substrate of the Umwelt, motor tremor as hydraulic interference, the temporal basis of conscious perception, and the coupled physical constraints that explain why large-diameter unmyelinated fibres do not exist in nature.

Keywords: nerve conduction; action potential; hydraulic wave; polyelectrolyte gel; Ling association-induction hypothesis; Donnan equilibrium; myelin; saltatory conduction; Hofmeister series; mechanoreceptor; Umwelt; Hodgkin-Huxley model

---

"Simplicity is the ultimate sophistication." —Leonardo da Vinci

"Everything should be made as simple as possible, but not simpler." —Albert Einstein

1. Introduction

The Hodgkin-Huxley (HH) equations, published in 1952, provide a quantitative description of the action potential that remains the foundation of computational neuroscience [3]. Their predictive power is not in question. What is in question is their physical interpretation. Hodgkin and Huxley were explicit on this point: "We do not wish to suggest that the equations we have used [...] necessarily bear any close relationship to the actual physical process involved." The equations are a phenomenological fit to data obtained from a specific preparation – the denudated giant squid axon with replaced axoplasm [4]. Baker, Hodgkin, and Shaw demonstrated that action potentials persist after axoplasm replacement with saline, and concluded, without further experimental tests, that the eliminated

 doi:10.20944/preprints202603.0725.v4

components were functionally neutral. The IMH model (Ionic-Mechano-Hydraulic: ionic gel phase transition as the primary event, mechanical compression as the trigger, and hydraulic wave propagation as the conduction mechanism) proposes that this conclusion was incorrect and that the cytoplasmic gel, structured water, adsorbed ions, and phase transitions eliminated by the preparation are the primary mechanism of conduction. We hereafter use the acronym IMH to emphasise the causal hierarchy: ionic desorption precedes and causes the mechanical and hydraulic events that follow.

The genealogy of the dominant model contains two earlier assumptions that deserve scrutiny. In 1902, Julius Bernstein applied the Nernst equation to quantify the resting membrane potential [2], on the advice of Wilhelm Ostwald. The Nernst equation is rigorously valid only for a single ion species, an ideal semipermeable membrane, under thermodynamic equilibrium [1] conditions, the axonal cytoplasm does not satisfy. This application was a convenient approximation that was never validated in the biological context; it was adopted and transmitted. The HH model inherits this unverified foundation.

A further structural issue concerns the preparation itself. Young (1936) established that the giant squid axon is not a single axon but a developmental fusion of hundreds of smaller axons [5], with an uncharacterised internal hydraulic architecture. The canonical preparation of twentieth-century electrophysiology was therefore neither structurally representative nor simple.

The present work does not propose to discard the HH model. It proposes to explain it: to identify the physical substrate from which its equations emerge as a first-order projection, and to provide the mechanistic account its authors called for. Section 2 describes the biophysical foundations of the IMH model. Section 3 presents convergent evidence from independent experimental observations. Section 4 states falsifiable predictions. Section 5 places the model in an evolutionary context. The Discussion and Conclusions assess the relationship between the two frameworks.

2. The IMH Model

2.1. The Cytoplasmic Gel: Ling's Foundation

Gilbert Ling demonstrated that the cytoplasm is a structured polyelectrolyte gel in which the majority of the intracellular K^+ is adsorbed at the protein sites rather than dissolved in a free solution [6]. The resting ionic distribution is a thermodynamically stable Donnan equilibrium, expressed in equation (1), where R is the gas constant, T the absolute temperature, F the Faraday constant, and the ratio in brackets is the K concentration gradient $^+$ across the gel boundary:

$$E_{\text{Donnan}} = -\frac{RT}{F} \ln\left(\frac{[K^+]_{\text{in}}}{[K^+]_{\text{out}}}\right) \tag{1}$$

Equation (1) differs from the Nernst equation in a critical respect: it describes a true thermodynamic equilibrium of the gel system as a whole, not a single-ion diffusion potential across an ideal membrane. This equilibrium is the energetically favourable state of the charged gel; it requires no metabolic pump to be maintained. Tamagawa formalised this framework in rigorous thermodynamic terms and quantitatively demonstrated that observed membrane potentials are consistent with Donnan equilibrium without pump-dependent gradient maintenance [7]. In this sense, the Na^+ / K^+-ATPase pump performs a regulatory and not a primary electrogenic function.

The adsorption of K^+ at gel sites follows a Langmuir isotherm, with affinity constants ordered by the Hofmeister ion series [8]. In equation (2), N is the total density of the adsorption sites, K_a is the adsorption affinity constant for K^+ and $[K^+]_{\text{free}}$ is the concentration of unbound K^+ in the gel interstitium:

$$[K^+]_{\text{ads}} = \frac{N \cdot K_a \cdot [K^+]_{\text{free}}}{1 + K_a \cdot [K^+]_{\text{free}}} \tag{2}$$

 doi:10.20944/preprints202603.0725.v4

Equation (2) has a direct physical consequence: when mechanical compression increases $[K^+]_{free}$ locally, the isotherm shifts and the adsorption sites become transiently saturated, releasing a pulse of free K^+ into the periaxonal space. This pulse is the ionic trigger of the hydraulic wave.

2.2. The Hydraulic Wave

Mechanical compression of the axon triggers the desorption of K^+ from the gel sites. Desorbed ions reconstruct their hydration shells, generating a local osmotic pressure gradient and hydraulic flux. A pressure wave propagates in the periaxonal space (12–15 nm width) at a velocity governed by the Korteweg-Moens equation adapted for a fluid-filled elastic tube of small radius:

$$v = \sqrt{\frac{K_{\text{eff}}}{\rho}} \tag{3}$$

$$K_{\text{eff}} = \left(\frac{1}{K_{\text{fluid}}} + \frac{2r}{E_{\text{myelin}} \cdot h} \right)^{-1} \tag{4}$$

where E_{myelin} is the elastic modulus of the myelin sheath, r is the radius of the periaxonal canal, h is the thickness of the sheath, K_{fluid} is the bulk modulus of the periaxonal fluid and ρ is its density. Equation (4) contains the central experimental prediction of the model: *the conduction velocity is determined by the elastic modulus of myelin, not by the density of the sodium channel.*

The Heimburg-Jackson thermodynamic soliton model established that the lipid membrane near a phase transition supports mechanically reversible wave propagation [9]. The IMH model integrates this as a component of a three-way thermal balance, expressed in equation (5), where the three terms represent respectively the heat absorbed by the membrane lipid phase transition, the heat released by K^+ resorption onto gel sites during recovery, and the heat exchanged with the structured water shell surrounding the desorbed ions.

$$\Delta Q_{\text{total}} = \Delta Q_{\text{lipid}} + \Delta Q_{\text{gel}} + \Delta Q_{\text{water}} \approx 0 \tag{5}$$

The near-zero net heat exchange measured during the action potential [11] is a thermodynamic constraint. Equation (5) satisfies it by construction, because the three contributions are thermodynamically coupled and partially cancel: what the membrane lipid phase transition absorbs, the gel recovery releases. The HH model, which is irreversible by design, does not account for this constraint.

2.3. The Universal Sigmoid as Gel Thermodynamics

Every known biological sensory receptor—mechanoreceptor, photoreceptor, nociceptor, thermoreceptor, and chemoreceptor—exhibits a sigmoidal stimulus-response curve. In the HH framework, this universality requires a separate molecular justification for each receptor class. In the IMH model, it is a necessary consequence of polyelectrolyte gel thermodynamics, expressed in equation (6), where $R(S)$ is the receptor response as a function of stimulus intensity S, R_{max} is the maximum response, $S_{\text{threshold}}$ is the activation threshold, and k is the slope parameter governing transition sharpness:

$$R(S) = \frac{R_{\text{max}}}{1 + e^{-k(S - S_{\text{threshold}})}} \tag{6}$$

Equation (6) is not fitted to receptor data post-hoc: its three parameters are determined independently by the physical properties of the gel. $S_{\text{threshold}}$ is the minimum compression for a self-sustaining hydraulic wave (a geometric condition of the periaxonal canal); k is the gel surface-to-volume ratio; and R_{max} is determined by the total density of the adsorption sites. The sigmoid emerges from gel thermodynamics, not from curve fitting. The diversity of receptors between species reflects the diversity of hydraulic architectures, not the diversity of molecular transduction mechanisms. This reformulates von Uexküll's Umwelt principle [14] in biophysical terms: the perceptual world of each species is the hydraulic geometry of its peripheral nervous system made accessible to it.

 doi:10.20944/preprints202603.0725.v4

2.4. The Axon-Schwann Cell Couple as Hydraulic Waveguide

The key architectural unit of the IMH model is not the axon in isolation but the axon-Schwann cell couple. Santiago Ramón y Cajal's neuron doctrine (1906), while correct regarding synaptic connectivity, imposed an analytical separation of the axon from its Schwann cell that made the periaxonal space conceptually invisible. The Schwann cell is not passive support: it provides the elastic wall of the hydraulic tube and contributes to the regulation of periaxonal ionic composition. Pannese documented the structural continuity of this couple in detail [15]. A century of electrophysiology conducted on the isolated axon –with the elastic wall removed, the periaxonal space disrupted, and the gel replaced – was conducted on half of the functional unit, without ever testing whether the other half was neutral.

3. Convergent Evidence

3.1. Huxley and Stämpfli 1949: The Anomaly That Was Named and Left Unexplained

In their study of saltatory conduction in the sciatic nerve of frogs, Huxley and Stämpfli recorded a result they described in their own words as "impossible in a resistance and capacity system [10]: a positive current entered the axis cylinder at node $N{+}1$ *before* the membrane potential at node N had reached its maximum. This directly contradicts the temporal logic of any RC-based propagation model, in which the downstream node can only be activated after the upstream node has completed depolarisation.

The arithmetic clarifies the constraint. For a frog sciatic nerve with conduction velocity $v = 60\,\mathrm{m/s}$ and internodal length $L = 1\,\mathrm{mm}$:

$$\Delta t_{N\to N+1} = \frac{L}{v} = \frac{1\times10^{-3}}{60} \approx 17\,\mu\mathrm{s} \tag{7}$$

The duration of the action potential at a single node is approximately 1 ms. Node $N{+}1$ therefore activates when node N has consumed only:

$$\frac{\Delta t}{\tau_{\mathrm{AP}}} = \frac{17\,\mu\mathrm{s}}{1000\,\mu\mathrm{s}} = 0.017 \tag{8}$$

That is, 1.7% of its duration of action potential. In the electrical model, this requires that node N generates sufficient axial current within 17 μs to depolarise node $N{+}1$ past the threshold, a demand inconsistent with the measured RC time constants of the nodal membrane. In the IMH model, the periaxonal pressure wave arrives at node $N{+}1$ in 17 μs independently of the electrical state of node N, because the wave is the primary event and the electrical response is its consequence. The 1949 anomaly is resolved without modification. This result is not specific to the sciatic nerve of the frog. For any myelinated fibre, the inter-nodal transit time $\Delta t_{N\to N+1} = L/v$ must be compared with the duration of the action potential τ_{AP} at a single node.

$$\frac{L}{v} < \tau_{AP} \tag{9}$$

Whenever node $N+1$ is activated before the action potential at node N is completed. This condition is satisfied by all fast myelinated fibres in vertebrates: for a human motor fibre with $v = 70$ m/s, $L = 10$ mm, and $\tau_{AP} \approx 1$ ms, one obtains $L/v \approx 0.14$ ms, well below τ_{AP}. More precisely, the fraction of the action potential that elapsed at node N when node $N+1$ is activated is $\Delta t/\tau_{AP} \approx 0.14$, which means that $N+1$ is triggered during the earliest rising phase of the action potential at N — before any significant depolarisation has propagated axially. The 1949 anomaly is therefore not an exception but the general rule of saltatory conduction. The RC model is structurally incompatible with physiological conduction velocities across the entire class of fast myelinated fibres. In the IMH model, this is not a paradox: the periaxonal pressure wave arrives at $N+1$ independently of the electrical state of N, because the wave is the primary event and the electrical response is its consequence.

 doi:10.20944/preprints202603.0725.v4

3.2. The RC Invariance Argument

In classical cable theory, $\tau = R_{\text{axial}} \cdot C_{\text{membrane}}$. Both resistance and capacitance scale with internodal length L, as shown in equation (10), where ρ_i is axoplasm resistivity, r is axon radius, c_m is specific membrane capacitance and L is internodal length:

$$R_{\text{axial}} = \frac{\rho_i L}{\pi r^2}, \qquad C_{\text{membrane}} = c_m \cdot 2\pi r \cdot L \tag{10}$$

Equation (10) shows directly that $\tau = R_{\text{axial}} \cdot C_{\text{membrane}}$ scales as L^2: doubling the internodal length doubles resistance and doubles capacitance, quadrupling the time constant. The apparent velocity gain attributed to increased internodal spacing in myelinated fibres is therefore an arithmetic artefact: the RC reduction from lower capacitance per unit length is exactly cancelled by a proportional resistance increase. Myelination cannot accelerate conduction through the electrical mechanism alone. The hydraulic model does not require such cancellation: the velocity is determined directly by E_{myelin} through equations (3) and (4).

3.3. Thermal Signatures of the Action Potential

Ichiji Tasaki documented over six decades a series of observations incompatible with the purely electrical model: longitudinal mechanical displacement of the myelin sheath coincident with the action potential, near-zero net heat exchange and anomalous bidirectional conduction results [11]. These observations were noted and set aside by the field for lack of a theoretical framework capable of integrating them. The IMH model provides this framework: Tasaki's longitudinal myelin displacement is the macroscopic surface signature of the periaxonal pressure wave. His thermal measurements satisfy equation (5).

Masson and Gallot (2008) provided a more recent and quantitatively rigorous treatment of thermal exchange during the action potential [12], using a statistical physics model of ionic and water effusion through membrane nano-channels. Their model predicts a temperature variation of approximately 22 μK for a 10 μm radius axon, in good agreement with experimental measurements [11]. Crucially, Masson and Gallot identified coupled water flux as a necessary component of the thermal account—a conclusion that converges independently on the IMH framework. However, their model remains within the interpretive structure of the HH: the effusion is trans-membranous, the channels are the primary actors, and the near-zero net thermal balance expressed in equation (5) is not addressed. The IMH model proposes the missing constraint: the three-way coupling of lipid, gel, and water contributions is the physical reason why the net exchange approaches zero—not a coincidence to be quantified after the fact.

3.4. The Cnidarian Nematocyst as Macroscopic Proof of Principle

The nematocyst of cnidarians demonstrates the ionic-hydraulic coupling mechanism on a directly measurable scale [13]. The organelle withstands an osmotic pressure of 150 bar, discharges in 700 ns, and produces an acceleration of 5.4×10^6 g. The trigger is Ca^{2+} desorption from a polyanionic capsule matrix, the same ionic-gel phase transition proposed for the periaxonal space in vertebrate axons, operating with measurable parameters. Cnidarians are among the first animals with a nervous system (>500 Myr), which established the ionic-hydraulic mechanism as evolutionarily ancient. The nematocyst is the bottom of the hydraulic fractal: the same principle operating at the nm– μm scale in 700 ns operates at the μ m scale in ms in the axon and at larger scales over longer time constants in the astrocytic syncytium and glymphatic system.

3.5. Axonal Mechanics: The Gel Identity of the Cytoskeleton

Independent biomechanical evidence for the gel nature of the interior of the axon was provided by Dubey et al. (2020), using a strain-controlled optical-fibre force apparatus in chick dorsal root ganglion axons [18]. The authors demonstrate three properties that are diagnostic of a polyelectrolyte gel rather than a simple viscous fluid or a microtubule cable: (i) the axon exhibits a *strain* softening response in

 doi:10.20944/preprints202603.0725.v4

which the steady-state elastic modulus decreases with increasing strain; (ii) the long-time behaviour is that of a *viscoelastic solid*, with a non-zero steady-state tension and memory of the initial state; (iii) the dominant mechanical contributor is not the microtubule bundle but the *actin-spectrin periodic lattice*, which buffers tension by reversible unfolding of the repeat domains of the spectrin.

These findings were obtained by researchers working entirely within the framework of biophysics and cytoskeletal mechanics, without reference to the HH model or nerve conduction. Their characterisation of the axonal cortex as a tension-buffering gel with solid-like long-time behaviour and strain-softening is precisely the material description required by the IMH model for the substrate that undergoes an ionic-hydraulic phase transition during the action potential. The convergence is independent and unintentional.

4. Predictions

4.1. Myelin Elastic Modulus and Conduction Velocity

Prediction: Conduction velocity in myelinated axons correlates with the elastic modulus E_{myelin} of the myelin sheath (measurable by atomic force microscopy in isolated fibres), independently of the channel density Na^+.

The HH model predicts that the velocity is determined by the kinetics and density of the channels. The IMH model predicts that it is determined by myelin rigidity via equations (3)–(4). The two predictions are orthogonal and experimentally separable. Demyelinating conditions that reduce E_{myelin} should slow conduction in proportion to $\sqrt{E_{\text{myelin}}}$, not in proportion to channel loss.

4.2. Mechanoreceptor Adaptation as Hydraulic Geometry

Prediction: Altering the fluid volume or viscosity of sensory corpuscles (Pacinian, Meissner, Krause end bulbs) without modifying receptor channel composition should shift the adaptation rate and frequency selectivity according to hydraulic equilibration time calculations derived from equation (4).

In the HH framework, adaptation is a property of channel kinetics. In the IMH model, it is a property of the hydraulic geometry of the corpuscle. The two models make quantitatively different predictions for the same viscosity manipulation.

4.3. Terminal Arborisations: Slowness as Geometric Amplifier of the Umwelt

Sensory terminal arborisations are the finest and slowest branches of the peripheral nervous system. Within the HH framework, this slowness is a physical limitation of small-diameter unmyelinated fibres. Within the IMH model, it is an evolutionary calibration: the temporal bandwidth of biologically relevant events determines the hydraulic geometry of the terminal arbour.

A punctate mechanical stimulus activates multiple terminal branches at different distances from the integration point of the arborisation, irrespective of fibre type. The resulting delays in arrival between branches encode the spatial geometry of the stimulus as a temporal signature, as expressed in equation (11), where L_i and L_j are the lengths of two terminal branches reaching the same receptive field point through different paths, and v_{terminal} is the hydraulic wave velocity in those branches:

$$\Delta t_{ij} = \frac{L_i - L_j}{v_{\text{terminal}}} \tag{11}$$

Equation (11) establishes the fundamental encoding principle: Δt_{ij} is the temporal delay between the two hydraulic messages reaching the integration point of the arborisation from the same stimulus point. This delay is a spatial coordinate transformed into a temporal one. *Slowness amplifies geometry.*

The motor arborisation inverts the principle: synchrony of muscle fibre contraction requires synchrony of hydraulic wave arrival at motor end-plates. Equal branch lengths produce simultaneous arrival and maximal impulsive force; unequal branch lengths produce staggered arrivals and temporally distributed force.

 doi:10.20944/preprints202603.0725.v4

Falsifiable prediction: The spatial resolution of a cutaneous receptor field correlates with the maximum branch length differential of its sensory arborisation, measurable by anatomical reconstruction. For motor units: the temporal profile of the compound EMG reflects terminal branch length distribution, distinguishable from predictions based on fibre conduction velocity alone.

4.4. Motor Tremor as Hydraulic Interference

Smooth motor fusion requires successive hydraulic waves to arrive at terminal arborisations in constructive temporal superposition. The critical firing frequency above which destructive interference produces tremor is given by equation (12), where $v_{\text{hydraulic}}$ is the hydraulic wave velocity in the terminal branches and $L_{\text{max branch}}$ is the length of the longest branch in the motor arborisation:

$$f_{\text{critical}} = \frac{v_{\text{hydraulic}}}{L_{\text{max branch}}} \tag{12}$$

Equation (12) provides a direct geometric interpretation of pathological tremor: if the firing frequency exceeds f_{critical}, successive hydraulic wavefronts arrive at terminal end-plates before the preceding wave has fully dissipated, producing destructive superposition and loss of smooth force summation. The three types of clinical tremor –Parkinsonian (4–6 Hz), essential (8–12 Hz), cerebellar (variable)—correspond to three distinct hydraulic regimes, each with a characteristic branch length distribution.

4.5. Composite Temporal Decoding and the Libet Latency

The peripheral nerve fibres span a conduction velocity range of 0.5–120 m/s. On a path length of 1 m, arrival delays range from 10 ms (Aα) to 1000 ms (C fibres). The Libet threshold of approximately 500 ms for conscious sensory perception is, in the IMH model, the minimum temporal integration window required to receive and decode the complete composite message, including its slow affective C-fibre component [16].

Prediction: Selective pharmacological blockade of C-fibre hydraulic transmission should abolish the subjective feel quality of a stimulus while preserving its fast discriminative component. Disruption of astrocytic gap junctions should selectively alter C-fibre signal integration while preserving fast-fibre processing [16].

4.6. Electrical Stimulation as Gel Trigger

The apparent success of external electrical field stimulation has been cited as evidence against purely mechanical models of nerve conduction. In the IMH model, this objection is resolved by the polyelectrolyte gel. An external electric field acts directly on the charged gel matrix and adsorbed ions, triggering the desorption electrically rather than mechanically. The same ionic-hydraulic phase transition is initiated; only the triggering stimulus differs.

Prediction: The threshold electric field for nerve stimulation correlates with the gel adsorption affinity constants (Hofmeister series position of the dominant adsorbed cation), not only with the membrane capacitance. This can be tested with gel-modifying agents that shift the adsorption affinity without altering the membrane electrical properties.

4.7. Non-Contamination Between Adjacent Fibres

Adjacent axons in a nerve bundle transmit distinct signals simultaneously without crosstalk. In the HH framework, the isolation is provided by myelin insulation. In the IMH model, each fibre is a sealed periaxonal canal; hydraulic waves cannot propagate between structurally independent tubes.

Prediction: Selective mechanical disruption of the periaxonal seal between two adjacent fibres—without affecting their electrical insulation—should produce hydraulic crosstalk detectable as correlated mechanical signals in both fibres simultaneously.

 doi:10.20944/preprints202603.0725.v4

4.8. Electromagnetic Dipole Geometry

A propagating hydraulic wavefront generates a moving ion desorption/resorption dipole along the axon, producing a propagating electromagnetic dipole rather than a stationary monopole.

Prediction: High-resolution EEG/MEG source modelling of single-fibre or small-fascicle signals should detect a dipolar electromagnetic signature progressing at hydraulic velocity, quantitatively distinguishable from the monopolar source geometry predicted by HH.

4.9. Axon Diameter Limits: Three Coupled Constraints

The IMH model predicts a set of coupled physical limits on axon diameter that jointly explain an otherwise unaccounted observation: large-diameter unmyelinated fibres do not exist in nature.

4.9.1. The Refractory Constraint in Unmyelinated Fibres

In the IMH model, the refractory zone is the length of the axon occupied by a propagating hydraulic wave that is still undergoing K^+ resorption at gel sites. As the axon diameter increases, the wave amplitude, conduction velocity, and refractory zone length all increase proportionally. The critical constraint is not on a single action potential but on the following one: successive impulses must not enter the refractory zone of the preceding wave. The maximum firing frequency is therefore inversely proportional to refractory zone length and, by extension, to axon diameter:

$$f_{\max} \propto \frac{1}{d} \tag{13}$$

where d is the diameter of the axon. A large-diameter unmyelinated fibre would be structurally limited to very low firing frequencies, rendering it functionally useless for information transmission at the signal bandwidths required by vertebrate nervous systems. The HH model does not offer a principled reason why large unmyelinated fibres should not exist; the IMH model predicts their absence from the energy and information-theoretic first principles.

4.9.2. The Ion Density Constraint

Maintaining a sufficient safety factor for hydraulic wave propagation requires a minimum density of adsorption sites (and, therefore, ion channels as secondary electromagnetic reporters) per unit of membrane area. As diameter increases, the gel volume and ion reservoir available per unit surface scale differently, eventually requiring a channel density that is metabolically and structurally untenable. This is the same constraint identified at the nanoscale in the companion paper [22]: the ionic reservoir is finite and scales unfavourably with the diameter for unmyelinated fibres.

4.9.3. The Amplitude-Velocity Trade-off and the Engineering Parallel

The biological constraint stands in instructive contrast to digital electronics. In semiconductor technology, the voltage amplitude has been systematically reduced – from 5 V in early microprocessors to below 1 V in modern architectures—because a lower amplitude enables faster switching: less charge to move, lower RC time constant, higher clock frequency. The nerve fibre faces the inverse constraint. In the IMH model, a larger amplitude hydraulic wave (requiring more ionic desorption, more channel activity, and more energy) is required to propagate faster or over a larger diameter. Biology cannot "lower the voltage" without losing propagation. This asymmetry defines a hard architectural ceiling on unmyelinated conduction speed.

4.9.4. Myelination as the Evolutionary Solution

The three above constraints converge on the same conclusion: beyond a critical diameter, unmyelinated fibres become simultaneously frequency-limited, energy-inviable, and amplitude-constrained. Myelination resolves all three by confining the hydraulic wave to the periaxonal canal at the Ranvier node, where the relevant geometry is the diameter and length of the node –not the full diameter of the

 doi:10.20944/preprints202603.0725.v4

internode. The node can be small while the internode is large, decoupling the amplitude requirement from the velocity requirement.

For myelinated fibres, two further constraints apply. First, the node length sets a minimum below which the ionic desorption event cannot sustain a self-propagating wave. Second, increasing the diameter of the fibre requires proportionally longer internodes to preserve the hydraulic impedance match at the node, imposing a geometric scaling law between the length of the internode, the geometry of the node and the thickness of the myelin.

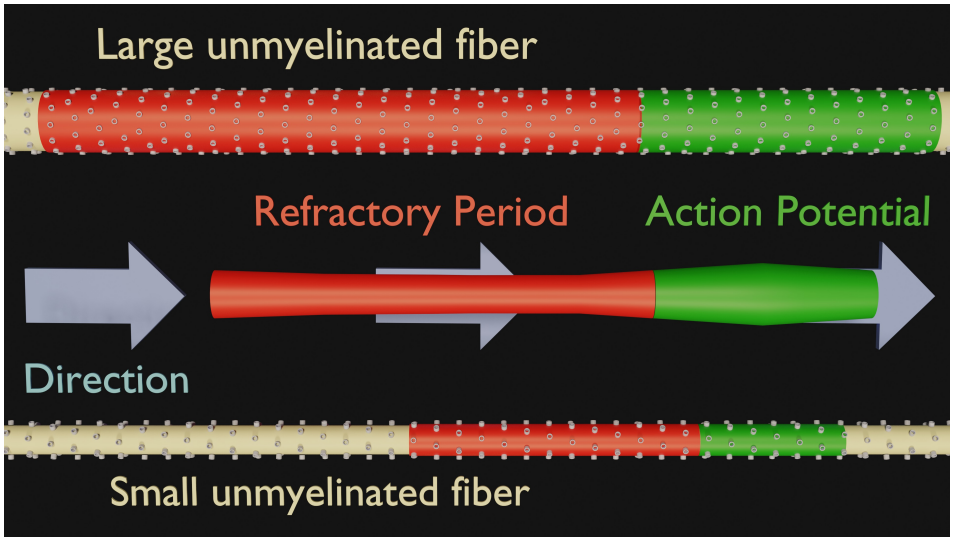

Figure 1. Refractory constraint and ion density as a function of axonal diameter in unmyelinated fibres. The propagating action potential (green) is followed by a refractory zone (red) in which K^+ resorption onto gel sites is still in progress and a second impulse cannot be sustained. *Top*: In a large-diameter unmyelinated fibre, the refractory zone occupies a proportionally greater length of the axon, severely limiting the maximum firing frequency ($f_{max} \propto 1/d$, equation 13); simultaneously, the gel volume scales as d^2 while the adsorption site density per unit surface area scales unfavourably, imposing the ion density constraint of Section 4.9.2. *Bottom*: In a small-diameter unmyelinated fibre, both constraints are satisfied: the refractory zone is short relative to axon length and the ion reservoir per unit surface remains adequate. The IMH model predicts that beyond a critical diameter ($d \approx 1.5\,\mu$m), large unmyelinated fibres become simultaneously frequency-limited and ionically inviable—explaining their absence from vertebrate nervous systems on physical, not developmental, grounds. The schematic also illustrates the proportionality between wave amplitude and fibre diameter: the hydraulic wavefront in the large fibre (centre) is broader and more energetically costly, imposing the amplitude–velocity trade-off discussed in Section 4.9.3.

Prediction: The upper diameter limit of unmyelinated fibres and the node-to-internode geometry of myelinated fibres should follow quantitative scaling laws derivable from equations (3)–(4) and the ion adsorption isotherm (2). Specifically: (i) the diameter of the unmyelinated fibre should be bounded by a critical value above which f_{max} falls below the minimum physiological firing rate of the fibre class; (ii) in myelinated fibres, the ratio of node length to internode length should correspond to the elastic modulus in the manner prescribed by equation (4).

4.9.5. Quantitative Velocity-Diameter Scaling and the Collapse Exponent

The three constraints above generate a characteristic velocity-diameter profile whose shape is quantitatively derivable from equations (3)–(4). Within the biologically viable range, myelinated fibres follow the empirically established linear relation $v \propto d$ [23,24]. This linearity is a direct consequence of the Korteweg-Moens equation under the anatomical constraint that myelin thickness scales proportionally with the diameter of the fibre (ratio $g \approx 0.6$, constant across the fibre classes [25]): since $h \propto d$ and the elastic modulus of a laminated cylindrical shell scales as $E_{myelin} \propto d^2$, equations (3) – (4) yield $v \propto d^1$ exactly. The parabolic relation $v \propto d^{1/2}$ predicted by cable theory [25] and empirically validated

 doi:10.20944/preprints202603.0725.v4

only by extrapolation to the giant squid axon, a composite fusion of hundreds of smaller axons [5] whose hydraulic architecture is uncharacterised, is not a prediction of the IMH model.

Beyond the anatomical limits ($d_{\max} \approx 20\,\mu$m for myelinated fibres; $d_{\max} \approx 1.5\,\mu$m for unmyelinated fibres), the IMH model predicts that effective conduction velocity does not continue to increase but collapses, following a power law with exponent $-3/2$:

$$v_{\text{eff}}(d) = v_{\max}\left(\frac{d_{\max}}{d}\right)^{3/2}, \quad d > d_{\max} \tag{14}$$

The exponent $3/2$ is not fitted but is derived from two independent physical contributions that combine multiplicatively. For myelinated fibres beyond $d_{\max}$: (i) the cost of ionic desorption scales as d^2 (gel volume), while (ii) the hydraulic driving pressure scales as d^{-1} by the Laplace relation $\Delta P = 2\gamma/r$; therefore, the ratio of available energy to required pressure decreases as d^{-3}, and since the velocity scales as the square root of this ratio in the Korteweg-Moens framework, the effective velocity declines as $d^{-3/2}$. For unmyelinated fibres beyond $d_{\max}$: without a confining myelin sheath, the hydraulic wave radiates cylindrically; the amplitude of a cylindrical wave decays as $r^{-1/2}$, and the wave can no longer sustain propagation when the amplitude falls below the gel desorption threshold. The combined effect of amplitude decay and increased gel volume again yields an effective velocity that decreases as $d^{-3/2}$.

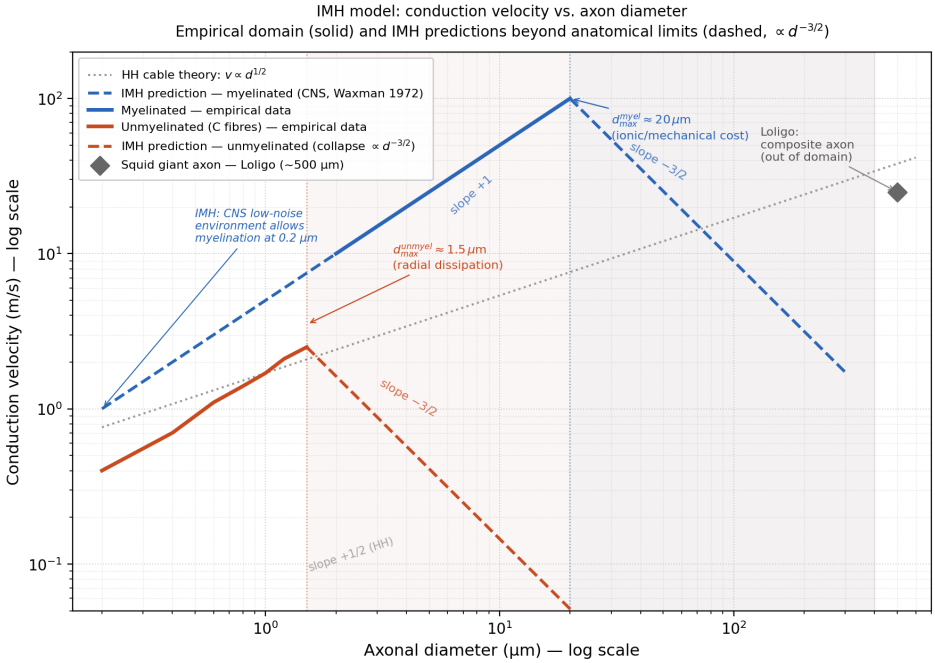

Figure 2. Conduction velocity as a function of axonal diameter: empirical data and IMH predictions (log–log scale). Solid lines show the empirically established velocity–diameter relations for myelinated fibres (blue, Hursh 1939; Waxman and Bennett 1972 [23]) and unmyelinated C fibres (red). Dashed lines extend each relation beyond the respective anatomical limits ($d_{\max}^{\text{myel}} \approx 20\,\mu$m; $d_{\max}^{\text{unmyel}} \approx 1.5\,\mu$m) according to the IMH collapse law (equation 14, exponent $-3/2$, derived from Korteweg–Moens mechanics). In log–log coordinates, the empirical linear relation $v \propto d^1$ (slope $+1$, blue solid) is a straight line, as is the collapse ($v \propto d^{-3/2}$, slope $-3/2$, blue and red dashed). The dotted grey line shows the Hodgkin–Huxley cable-theory prediction $v \propto d^{1/2}$ (slope $+1/2$, Rushton 1951), which continues to rise without bound and predicts conduction in arbitrarily large unmyelinated fibres—a prediction contradicted by anatomy. The diamond marker indicates the squid giant axon (*Loligo*, $d \approx 500\,\mu$m, $v \approx 25$ m/s), which lies far outside the biological domain of individual axons and whose inclusion by Rushton to validate the $v \propto d^{1/2}$ relation is critiqued in Section 6. The two models diverge maximally in the zone 2–50 μm for unmyelinated fibres, where the IMH predicts collapse and HH predicts continued acceleration—a range directly accessible to experiment.

 doi:10.20944/preprints202603.0725.v4

The lower end of the myelinated range is provided by Waxman and Bennett [23], who demonstrated that in the central nervous system, myelinated fibres with diameters as small as 0.2 μm conduct faster than unmyelinated fibres of the same diameter–directly contradicting the Rushton critical-diameter argument (which predicts that myelination ceases to accelerate conduction below $\sim 1\,\mu$m) and confirming the linear relation $v \propto d$ at the small-diameter end. Within the IMH framework, this observation is explained by the noise properties of the CNS environment: the periaxonal space is hydraulically better confined (blood-brain barrier, glial envelope, cerebrospinal fluid cushion) than the peripheral nerve, so the minimum wave amplitude required for reliable propagation is lower, and the linear regime extends to smaller diameters. The minimum myelinated fibre diameter is not a universal constant, but an environmental noise floor.

5. Evolutionary Perspective

The gel generating hydraulic pressure in a confined space operates recursively across at least five biological scales: nematocyst (nm–μm, ns) [13], periaxonal axonal space (μm, ms), dendritic arborisations (mm, tens of ms), astrocytic syncytium (cm, s) and glymphatic system (organ, circadian). The fractal geometry of neural arbors, from terminal arborisations to dendritic trees to cortical columns, may be the spatial imprint of this temporal recursion.

The Heimburg-Jackson soliton model [9] converges to the IMH framework from membrane thermodynamics: both models require reversible mechanical wave propagation and near-zero net heat exchange. The two frameworks are complementary, addressing different physical levels of the same phenomenon.

Damasio's identification of C fibres as the primary substrate of felt experience [16] provides an independent clinical convergence: the slow peripheral hydraulic message arriving last is the affective dimension of perception, not noise. Descartes attributed neural function to hydraulic spirits; Damasio rediscovered the role of slow peripheral signals through clinical observation; the IMH model provides the biophysical substrate.

6. Discussion

The IMH model does not falsify the HH equations. It explains them. The HH model accurately describes the electrical correlates of the action potential in a preparation that has removed the gel, the periaxonal space, the Schwann cell, and mechanical coupling from the measurement. In those conditions, the electrical description is correct and complete. The IMH claim is that these conditions do not describe physiological nerve conduction and that the physical process in the intact fibre has a hydraulic primary layer that the HH electrical measurements capture only as a projection.

Barz et al. (2013) proposed a purely mechanical pressure-wave model in which ion channels are pressure-gated rather than voltage-gated [17]. That model correctly identified the wave as primary but lacked ionic-gel coupling: it had no threshold mechanism, no sigmoid, no ionic selectivity, and no account of electrical stimulation. The IMH model provides the missing components through the Ling-Tamagawa polyelectrolyte gel framework. The elementary molecular mechanism by which a single membrane protein converts ion binding energy into hydraulic work is formalised in a companion paper [29], which proposes the V→U membrane actuator as the evolutionarily ancestral motor underlying the ionic-hydraulic phase transition and identifies Ca^{2+} as the orchestrator of the reset cycle that defines both the absolute and relative refractory periods.

The need for such an extension is recognised within mainstream modelling. Peets, Tamm, and Engelbrecht (2023), reviewing the state of mathematical models of nerve signal propagation, explicitly call for the incorporation of the cytoskeleton as a potentially primary actor, citing evidence that its removal alters the response to axoplasmic pressure by an order of magnitude [19]. They concluded that the cytoskeleton could prove "as important for signal propagation in nerves as the cell membrane." The IMH model answers this call.

 doi:10.20944/preprints202603.0725.v4

The theoretical positioning of the present model within the broader landscape of non-HH frameworks is clarified by Drukarch and Wilhelmus (2023), who distinguish two approaches to the multiphysics of the nerve signal: a bottom-up mechanistic approach that retains HH as the driving layer and adds mechanical coupling as an epiphenomenon, and a top-down thermodynamic approach that treats the nerve signal as emerging from the collective physics-chemical properties of the axolemma-ectoplasm complex [21]. The IMH model belongs unambiguously to the second category. Drukarch and Wilhelmus, moreover, provide an extensive treatment of Tasaki's gel phase transition framework — the bistable Ca^{2+}/Na^{+} ectoplasmic gel, volume phase transition, cooperative ion exchange, and refractory period as re-compaction kinetics — which constitutes the direct conceptual precursor of the ionic-gel layer of the present model. Their conclusion, that neuroscience "should welcome and be open to different perspectives on modelling and explanatory understanding of the physics of the nerve signal," applies directly to the present work, and their publication in a mainstream peer-reviewed venue signals that this openness is no longer confined to the margins of the field.

Independent philosophical support for this positioning is provided by Carrillo (2024), whose survey of models of the nerve impulse in the *Routledge Handbook of Philosophy of Scientific Modeling* explicitly frames the contrast between the Hodgkin–Huxley model and thermodynamic alternatives in terms of Einstein's distinction between constructive (bottom-up) and first-principle (top-down) theories [20]. Carrillo notes that "very little philosophical discussion has appeared" on the implications of this controversy—a lacuna that the present work addresses from the mechanistic side. Notably, Carrillo's survey covers Tasaki's macromolecular model and the Heimburg–Jackson soliton framework but does not include the polyelectrolyte gel layer (Ling–Tamagawa–Matveev), which constitutes the ionic substrate common to both. The absence of this framework from the philosophical literature reflects its marginalisation within mainstream electrophysiology rather than any evidence deficiency and points to a gap that the IMH model is positioned to fill.

An additional convergence deserves explicit recognition. Manoj and Jaeken (2023), proposing the murburn concept as a unifying framework for cellular bioenergetics, situate Ling's association-induction hypothesis as a foundational precursor shared by several non-classical schools, and cite Tamagawa and Matveev directly as contemporary representatives of this tradition [26]. Tamagawa is himself a co-author of two murburn electrophysiology papers, one providing a critical comparative analysis of the membrane-pump and association-induction frameworks [27], and one repositioning Na^{+} / K^{+}-ATPase as a thermodynamic equilibrium facilitator rather than an active electrogenic pump [28]—a conclusion that directly corroborates the regulatory, non-primary role assigned to the pump in Section 2.1 of the present work. The murburn framework, centred on diffusible reactive species (DRS) as primary agents of ATP synthesis and cellular coherence, addresses the bioenergetic layer that the present model does not treat explicitly. The two frameworks are complementary rather than competing: the IMH model describes the propagation physics of the nerve signal, while the murburn framework addresses the metabolic resetting that restores the gel to its adsorption-competent state between impulses. In this reading, the refractory period acquires a biochemical correlate, DRS–mediated gel recompaction, that is absent from both HH and purely mechanical wave models. Ling's polyelectrolyte gel thus serves as a common substrate linking bioenergetics (murburn), resting potential (Donnan-Tamagawa) and propagation (the present model): three aspects of a single physical object seen from three disciplinary vantage points.

The principal limitation of the present work is theoretical: the model has not yet been subjected to systematic quantitative fitting against the full HH dataset. Equations (3) – (4) yield numerical predictions for conduction velocity as a function of measurable mechanical parameters (E_{myelin}, r, h), but these predictions have not yet been compared quantitatively against the extensive velocity-diameter dataset available for vertebrate nerve fibres. This comparison is a necessary next step.

A second limitation concerns the preparation of the giant squid axon. Because this axon is a fusion of hundreds of smaller axons [5], its hydraulic architecture is unknown. The HH data set, obtained on this preparation, cannot straightforwardly constrain a hydraulic model designed for single-axon

 doi:10.20944/preprints202603.0725.v4

geometry. A purpose-designed experimental protocol is required on single myelinated mammalian fibres with intact periaxonal space.

7. Conclusions

The IMH model proposes that the action potential is a coupled ionic-hydraulic phase transition in which mechanical compression triggers K^+ desorption from cytoplasmic gel sites, generating a pressure wave in the periaxonal space. Electrical events are the measurable consequence of this wave, not its cause. The model resolves, without post-hoc adjustment, the 75-year anomaly of Huxley and Stämpfli (1949) [10], accounts for the nearly zero net heat exchange of the action potential [11], and provides a unified physical basis for the universal sigmoidal stimulus-response curve of biological sensors.

Nine falsifiable predictions are presented, each testable with existing or near-existing experimental methods. The model is falsified if the conduction velocity in the myelinated fibres is found to be independent of the elastic modulus of myelin, if the adaptation rates of mechanoreceptors are not affected by corpuscle fluid manipulation, if the lengths of the terminal arborization branch are not correlated with the spatial resolution of the receptor field, or if the velocity-diameter relation departs from $v \propto d^1$ (rather than the cable prediction $v \propto d^{1/2}$) when measured in intact fibres with preserved periaxonal space.

The Hodgkin-Huxley model served seven decades with distinction. The IMH model does not request its rejection. It asks for the experiment.

Preceding Work

This manuscript extends and contextualises an earlier study by the same authors:
Delalande, B.; Tamagawa, H.; Matveev, V. From Nernst to Bernstein and Beyond. *Preprints* **2020**, 2020080529. doi:10.20944/preprints202008.0529.v2

Author Contributions: Conceptualisation: B.D., H.T., V.M. Theoretical framework and formal analysis: B.D. and V.M. (polyelectrolyte gel foundations), B.D. and H.T. (hydraulic wave mechanics). Writing—original draft: B.D. Writing—review and editing: H.T. and V.M. All authors have read and agreed to the submitted version of the manuscript.

Funding: This research did not receive external funding.

Use of Artificial Intelligence: The authors used large language model (LLM) assistants (Claude, Anthropic) during the preparation of this manuscript for tasks that included literature search, LaTeX editing, and paragraph writing. All scientific content, theoretical claims, and conclusions are the sole responsibility of the authors. The authors have reviewed and verified all AI-assisted content.

Acknowledgments: The intellectual genealogy of this work begins with SomaSimple, a forum created by the first author where clinicians and researchers daily faced the dissonance between classical electrophysiology and living patients. SomaSimple was the space in which the question was first posed clearly: if the HH model is correct, why does clinical neuroscience fail so consistently to predict the behaviour of the living nervous system? It was on ResearchGate, however, that the exchanges proved most scientifically fertile: Vladimir Matveev deposited his work on Ling's gel theory there, introducing the first author to a framework capable of answering the question SomaSimple had raised. ResearchGate also provided the channel through which the connection with Hirohisa Tamagawa was established and through which sustained exchanges with Ennio Pannese (1928–2025) and Thomas Heimburg enriched the model's anatomical and thermodynamic foundations. The authors thank Ennio Pannese in particular, whose meticulous neurocytological documentation of the axon-Schwann cell couple informed Section 2.4, and who responded to detailed anatomical queries with generosity and precision up to the end of his life.

Conflicts of Interest: The authors declare no conflicts of interest.

 doi:10.20944/preprints202603.0725.v4

References

1. Nernst, W. Zur Kinetik der in Lösung befindlichen Körper. *Z. Phys. Chem.* **1888**, *2*, 613–637.
2. Bernstein, J. Untersuchungen zur Thermodynamik der bioelektrischen Ströme. *Pflügers Arch.* **1902**, *92*, 521–562.
3. Hodgkin, A.L.; Huxley, A.F. A quantitative description of membrane current and its application to conduction and excitation in nerve. *J. Physiol.* **1952**, *117*, 500–544.
4. Baker, P.F.; Hodgkin, A.L.; Shaw, T.I. Replacement of the axoplasm of giant nerve fibres with artificial solutions. *J. Physiol.* **1962**, *164*, 330–354.
5. Young, J.Z. Structure of nerve fibres and synapses in some invertebrates. *Cold Spring Harb. Symp. Quant. Biol.* **1936**, *4*, 1–6.
6. Ling, G.N. *A Physical Theory of the Living State*; Blaisdell: New York, NY, USA, 1962.
7. Tamagawa, H.; Morita, S. Membrane potential generated by ion adsorption. *Membranes* **2014**, *4*, 257–274.
8. Hofmeister, F. Zur Lehre von der Wirkung der Salze. *Arch. Exp. Pathol. Pharmakol.* **1888**, *24*, 247–260.
9. Heimburg, T.; Jackson, A.D. On soliton propagation in biomembranes and nerves. *Proc. Natl. Acad. Sci. USA* **2005**, *102*, 9790–9795.
10. Huxley, A.F.; Stämpfli, R. Evidence for saltatory conduction in peripheral myelinated nerve fibres. *J. Physiol.* **1949**, *108*, 315–339.
11. Tasaki, I.; Iwasa, K. Rapid mechanical and thermal changes in the garfish olfactory nerve associated with a propagated impulse. *Biophys. J.* **1982**, *36*, 1–10.
12. Masson, J.-B.; Gallot, G. A model for thermal exchange in axons during action potential propagation. *Eur. Biophys. J.* **2008**, *37*, 1001–1006. doi:10.1007/s00249-008-0329-5.
13. Özbek, S.; Balasubramanian, P.G.; Holstein, T.W. Cnidocyst structure and the biomechanics of discharge. *Toxicon* **2009**, *54*, 1038–1045. doi:10.1016/j.toxicon.2009.03.006.
14. von Uexküll, J. *Umwelt und Innenwelt der Tiere*; Springer: Berlin, Germany, 1909.
15. Pannese, E. *Neurocytology: Fine Structure of Neurons, Nerve Processes and Neuroglial Cells*; Thieme: Stuttgart, Germany, 1994.
16. Damasio, A. *Feeling and Knowing*; Pantheon Books: New York, NY, USA, 2021.
17. Barz, H.; Schreiber, A.; Barz, U. Impulses and pressure waves cause excitement and conduction in the nervous system. *Med. Hypotheses* **2013**. PMID: 23953966.
18. Dubey, S.; Bhembre, N.; Bodas, S.; Ghose, A.; Callan-Jones, A.; Pullarkat, P.A. The axonal actin-spectrin lattice acts as a tension buffering shock absorber. *eLife* **2020**, *9*, e51772. doi:10.7554/eLife.51772.
19. Peets, T.; Tamm, K.; Engelbrecht, J. On mathematical modeling of the propagation of a wave ensemble within an individual axon. *Front. Cell. Neurosci.* **2023**, *17*, 1222785. doi:10.3389/fncel.2023.1222785.
20. Carrillo, N. Models of the nerve impulse. In *The Routledge Handbook of Philosophy of Scientific Modeling*; Routledge: London, UK, **2024**; pp. 549–560. doi:10.4324/9781003205647-46
21. Drukarch, B.; Wilhelmus, M.M.M. Thinking about the action potential: the nerve signal as a window to the physical principles guiding neuronal excitability. *Front. Cell. Neurosci.* **2023**, *17*, 1232020. doi:10.3389/fncel.2023.1232020.
22. Delalande, B.; Tamagawa, H.; Matveev, V. Physical inconsistencies in the Hodgkin-Huxley model at the nanoscale. *Preprints* **2026**, 2026030870. doi:10.20944/preprints202603.0870.v1
23. Waxman, S.G.; Bennett, M.V.L. Relative conduction velocities of small myelinated and non-myelinated fibres in the central nervous system. *Nature New Biol.* **1972**, *238*, 217–219.
24. Hursh, J.B. Conduction velocity and diameter of nerve fibers. *Am. J. Physiol.* **1939**, *127*, 131–139.
25. Rushton, W.A.H. A theory of the effects of fibre size in medullated nerve. *J. Physiol.* **1951**, *115*, 101–122.
26. Manoj, K.M.; Jaeken, L. Synthesis of theories on cellular powering, coherence, homeostasis and electromechanics: Murburn concept & evolutionary perspectives. *J. Cell. Physiol.* **2023**, *238*, 931–953. doi:10.1002/jcp.31000.
27. Manoj, K.M.; Tamagawa, H. Critical analysis of explanations for cellular homeostasis and electrophysiology from murburn perspective. *J. Cell. Physiol.* **2021**, *237*, 421–435. doi:10.1002/jcp.30578.

 doi:10.20944/preprints202603.0725.v4

28. Manoj, K.M.; Gideon, D.A.; Bazhin, N.M.; Tamagawa, H.; Nirusimhan, V.; Kavdia, M.; Jaeken, L. Na,K-ATPase: A murzyme facilitating thermodynamic equilibriums at the membrane-interface. *J. Cell. Physiol.* **2023**, *238*, 109–136. doi:10.1002/jcp.30925.
29. Delalande, B.; Tamagawa, H.; Matveev, V. Molecular Foundations of the IMH Model: The V→U Membrane Actuator. *Preprint* **2026**. doi:10.5281/zenodo.19159360